Title: Impacts of the Direct Radiative Effect of Aerosols in Numerical Weather Prediction over Europe Using the ALADIN-HIRLAM NWP System

Author(s): Toll, V., E. Gleeson, K.P. Nielsen, A. Männik, J. Mašek, L. Rontu, and P. Post.

Citation: Toll, V., E. Gleeson, K.P. Nielsen, A. Männik, J. Mašek, L. Rontu, and P. Post. "Impacts of the Direct Radiative Effect of Aerosols in Numerical Weather Prediction over Europe Using the ALADIN-HIRLAM NWP System." *Atmospheric Research* 172–173 (2016): 163–173. doi:10.1016/j.atmosres.2016.01.003.

Impacts of the direct radiative effect of aerosols in numerical weather prediction over Europe using the ALADIN-HIRLAM NWP system

V. Toll[a,b,*], E. Gleeson[c], K.P. Nielsen[d], A. Männik[a,b], J. Mašek[e], L. Rontu[f], P. Post[a]

[a] *University of Tartu, Tartu, Estonia*
[b] *Estonian Environment Agency (formerly EMHI), Tallinn, Estonia*
[c] *Met Éireann, Dublin, Ireland*
[d] *Danish Meteorological Institute, Copenhagen, Denmark*
[e] *Czech Hydrometorological Institute, Prague, Czech Republic*
[f] *Finnish Meteorological Institute, Helsinki, Finland*

Abstract

Aerosol feedbacks are becoming more accepted as physical mechanisms that should be included in numerical weather prediction models in order to improve the accuracy of the weather forecasts. The default set-up in the Aire Limitee Adaptation dynamique Developpement INternational (ALADIN) - High Resolution Limited Area Model (HIRLAM) numerical weather prediction system includes monthly aerosol climatologies to account for the average direct radiative effect of aerosols. This effect was studied using the default aerosol climatology in the system and compared to experiments run using the more up-to-date Max-Planck-Institute Aerosol Climatology version 1 (MACv1) climatology, and time-varying aerosol data from the Monitoring Atmospheric Composition and Climate (MACC) reanalysis aerosol dataset. Accounting for the direct radiative effect using monthly aerosol climatologies or near real-time aerosol distributions improved the accuracy of the simulated radiative fluxes and temperature and humidity forecasts in the lower troposphere. However, the dependency of forecast meteorological conditions on the aerosol dataset itself was found to be weak.

Keywords: numerical weather prediction, aerosol direct radiative effect, ALADIN-HIRLAM system, MACC reanalysis, MACv1 aerosol climatology.

*Corresponding author. Institute of Physics, University of Tartu, Ravila 14c, 51010, Tartu, Estonia. Tel.: +37253951001. E-mail address: velle.toll@ut.ee (V. Toll).

1. Introduction

The direct radiative effect of aerosols resulting from absorption and scattering of solar and terrestrial radiation alters the radiation budget of the Earth and has been widely studied to date (e.g. Haywood and Boucher, 2000; Bellouin et al., 2005; Jacobson et al., 2001; Myhre et al., 2013; Garcıa et al., 2012; Yu et al., 2006; Loeb and Manalo-Smith, 2005) with estimations improving in time (e.g. Myhre et al., 2013). It has considerable impacts on meteorology (e.g. Cook and Highwood, 2004; Takemura et al., 2005; Wang, 2004) which need to be accounted for to accurately simulate the Earth's climate.

Hohenegger and Vidale (2005) and Zubler et al. (2011) demonstrated the dependence of simulated regional climate on the direct radiative effect of aerosols over Europe. Both studies show noticeable sensitivity of the radiative fluxes and temperatures to the aerosol climatology used in the regional simulations. In the study presented here the impacts of the direct radiative effect of aerosols in short-range numerical weather prediction (NWP) forecasts using the Aire Limitee Adaptation dynamique Developpement INternational (ALADIN) - High Resolution Limited Area Model (HIRLAM) NWP system are studied. Numerical weather forecasts over a limited area, as opposed to climate simulations, are characterised by short forecast lead-times (up to few days) and constraints on the initial conditions through the assimilation of meteorological observations.

It is common to use monthly aerosol climatologies in NWP models. By default the ALADIN-HIRLAM system uses the monthly aerosol climatology described in Tegen et al. (1997) referred to as the TEG97 climatology hereafter. Tompkins et al. (2005) demonstrated the improved forecast of the African Easterly Jet in the European Centre for Medium-Range Weather Forecasts (ECMWF) global Integrated Forecast System (IFS) model as a result of using TEG97 instead of the previous fixed average aerosol distribution of Tanre et al. (1984) for calculating the direct radiative effect of aerosols. Rodwell and Jung (2008) also showed how this change in aerosol climatology led to improved forecasts and reduced seasonal-mean errors globally in the IFS model. However, when accounting for the direct radiative effect of real-time aerosol distributions rather than climatological distributions, the quality of the weather forecasts can be further improved. For example, Toll et al. (2015) showed considerable improvement in forecasts of near-surface conditions by the ALADIN-HIRLAM

system during Russian wildfires in summer 2010 when the direct radiative effect of realistic aerosol distributions was included. In addition, Palamarchuk et al. (2016) showed noticeable sensitivity in the simulated meterological parameters in the ALADIN-HIRLAM NWP system to the treatment of aerosols.

Not accounting for the direct radiative effect of aerosols based on realistic aerosol distributions can lead to considerable errors in the meteorological forecasts (Milton et al., 2008; Carmona et al., 2008). Coupled modelling of weather and air quality (Grell and Baklanov, 2011; Baklanov et al., 2014; Zhang, 2008) has been proposed as a possible way to improve weather forecasts, although the added computational cost for operational NWP must be weighted against the improvements in the results. According to Mulcahy et al. (2014) considering the influence of prognostic aerosols in NWP results in an improved radiation budget. However, they also showed that the influence on large-scale atmospheric circulation is generally weak in short-range forecasts. Reale et al. (2011) showed that although interactive aerosols in the National Aeronautics and Space Administration (NASA) Goddard Earth Observing System (GEOS) global model did not improve the 500 hPa height anomaly correlation scores, the representation of the African easterly jet was improved. Pérez et al. (2006) demonstrated an improvement in atmospheric temperature and mean sea-level pressure (MSLP) forecasts as a result of taking the radiative effects of mineral dust into account. According to Morcrette et al. (2011) using prognostic aerosols in the experimental set-up of ECMWF's IFS system has considerable regional effects on near-surface conditions, although the impacts on NWP verification scores are weak.

In addition to the influence on the accuracy of the NWP forecast, accurate simulation of the direct radiative effect of aerosols in the model is important when using simulated shortwave (SW) fluxes for solar energy applications. Breitkreuz et al. (2009) explained that during clear-sky conditions aerosols are the main modulator of the SW fluxes. Accounting for the direct radiative effect of aerosols properly improves the forecast of SW fluxes. Zamora et al. (2005) showed that when the aerosol optical depth (AOD) is larger than 0.1 errors in the simulated SW fluxes in NWP models of the order of 100 W/m^2 may occur, but for smaller AODs accounting for the climatological average direct radiative effect of aerosols gives an accurate estimate of SW fluxes. Ruiz-Arias et al. (2014) presented improved simulations of

surface SW fluxes using the Weather Research and Forecasting (WRF) NWP model by using a simple parametrization of the direct radiative effect of aerosols. This was based on 550 nm AOD and a knowledge of the type of the predominant aerosol.

The main goal of this paper is to evaluate the impact of considering the direct radiative effect of aerosols in ALADIN-HIRLAM short-range weather forecasts over Europe using input from different aerosol datasets. Climatological aerosol data from TEG97 and from the more up-to-date Max-Planck-Institute Aerosol Climatology version 1 (MACv1) (Kinne et al., 2013) is used as well as time-varying aerosol data from the Monitoring Atmospheric Composition and Climate (MACC) reanalysis (Inness et al., 2013) to determine the sensitivity of meteorological forecasts to the aerosol datasets. The aerosol datasets and the setup of the ALADIN-HIRLAM system are described in section 2. The modelling results are presented and compared to observations in section 3. The results and benefits of including the direct radiative effect of aerosols are discussed in section 4 and conclusions are drawn in section 5.

2. Data and methods

2.1. Aerosol datasets

2.1.1. Default aerosol climatology in the ALADIN-HIRLAM system (TEG97)

By default monthly averages of 550 nm AOD for dust, sulphates, sea salt, black carbon and organic matter from the TEG97 climatology are used in the ALADIN-HIRLAM system to calculate the direct radiative effect of aerosols. The horizontal resolution of TEG97 is 4° by 5°. This aerosol climatology is based on a combination of model results from different aerosol transport models for dust, sulphates, sea salt and carbonaceous aerosols (Tegen et al., 1997).

Zubler et al. (2011) found that AOD is a little lower over Europe in TEG97 compared to more recent aerosol climatologies, but is still adequate for considering the direct radiative effect of average aerosol distributions. In addition, regional aerosol distributions (e.g. dust over Northern Africa) have been found to be poorly represented in TEG97 due to the coarse resolution of the dataset (Nabat et al., 2013).

2.1.2. MACv1 aerosol climatology

The MACv1 aerosol climatology (Kinne et al., 2013) is based on high quality Aerosol Robotic Network (AERONET) (Holben et al., 1998) data fitted to the median aerosol from Aerosol Comparisons between Observations and Models (AeroCom). In phase 1 of AeroCom AOD data were provided by 14 models, from which the median was extracted by Kinne et al. (2013). They fitted data from each AERONET station to the AeroCom model background using quality and range scores for each AERONET site.

The horizontal resolution of this aerosol dataset is 1° by 1° (Kinne et al., 2013). Monthly climatological distributions of the total AOD combinig different aerosol species have been used. This climatology includes optical properties of aerosols for the years 1860 to 2100; in this study the optical properties for current conditions were used.

2.1.3. MACC reanalysis

The MACC reanalysis (Inness et al., 2013) was compiled using the IFS-MOZART model (Flemming et al., 2009) which combines a forward model (Morcrette et al., 2009) and the assimilation of satellite atmospheric composition data (Benedetti et al., 2009). It includes a reanalysis of reactive gases, aerosols and greenhouse gases. Regarding aerosols, AOD sensitive radiances from Moderate-resolution Imaging Spectroradiometer (MODIS) have been assimilated (Benedetti et al., 2009).

The horizontal resolution of this reanalysis dataset is approximately 80 km (Inness et al., 2013) with data available for the years 2003-2012. The concentrations of the following aerosol species are available in the dataset: sea salt, dust, organic matter, black carbon and sulphates.

2.2. Description of the NWP system

Experiments were carried out using a configuration of the ALADIN-HIRLAM system which combines hydrostatic dynamics with the so-called ALARO-0 physical parametrizations (Gerard et al., 2009). The latter is applicable at horizontal resolutions where convection needs to be fully parametrized (i.e. the case here) and across the so-called grey-zone where deep convection becomes partially resolved, down to kilometre resolutions where deep convection is fully resolved. The model can also be used for regional climate simulations (Lindstedt

et al., 2015), where the direct radiative effect of aerosols can be of even greater importance than in the short-range NWP runs studied here.

In the used configuration, the system of hydrostatic primitive equations is formulated on a conformal map using the terrain following, pressure-based hybrid eta-coordinates introduced by Simmons and Burridge (1981). The horizontal discretization employs bi-Fourier expansion with an artificial extension zone following Haugen and Machenhauer (1993) to make the fields biperiodic. The vertical discretization uses the finite element method of Untch and Hortal (2004). Temporal discretization is done using the two-time level semi-implicit scheme with semi-Lagrangian treatment of advection terms (Temperton and Staniforth, 1987; Hortal, 2002). Short-scale noise is controlled by the non-linear numerical diffusion of Váňa et al. (2008) which exploits the damping properties of semi-Lagrangian interpolators. Lateral boundary conditions are imposed via the Davies (1976) relaxation scheme.

Except for the radiation and surface schemes, the ALARO-0 physical parametrizations was used. ALARO-0 uses the flux-conservative governing equations of Catry et al. (2007), the pseudo-prognostic Turbulent Kinetic Energy (TKE) scheme of Geleyn et al. (2006) and a cloudiness scheme based on the Xu-Randall approach (Xu and Randall, 1996). Shallow convection is treated by the turbulence scheme, while the moist deep convection is treated within the so-called Modular Multi-scale Microphysics and Transport (3MT) scheme of Gerard et al. (2009), which handles both resolved and subgrid condensations by a single call to microphysics embedded between updraft and downdraft computations. The Kessler type one momentum microphysical scheme is used with statistical sedimentation of precipitation according to Geleyn et al. (2008). Mountain drag due to the subgrid scale orography is parametrized by the Catry et al. (2008) scheme.

Surface processes are parametrized by the SURFEX scheme of Masson et al. (2013). Radiation parametrizations correspond to an old configuration (cy25) of the IFS radiation scheme (White, 2004; Mascart and Bougeault, 2011). The SW scheme follows Fouquart and Bonnel (1980), but is extended to six spectral bands (0.185-0.25-0.44-0.69-1.19-2.38-4.00 μm). It employs the delta-Eddington approximation of Joseph et al. (1976). The performance of this scheme with respect to reference DISORT computations (Stamnes et al., 1988) was evaluated by Nielsen et al. (2014), and found to be highly accurate. The longwave (LW)

radiation scheme is the RRTMG-LW scheme of Mlawer et al. (1997), which was developed as an economical scheme that closely matches the LBLRTM reference (Clough et al., 2005) scheme. It is based on the correlated k-distribution method and has 16 spectral bands and 140 g-intervals. LW scattering is neglected in this scheme.

Only the direct radiative effect of aerosols is considered in this study. Climatological vertical profiles of aerosols are assumed, with attenuation coefficients decaying exponentially with height (Tanre et al., 1984). The AOD at a wavelength of 550 nm is used as input to the radiation scheme. The AOD for each SW and LW spectral interval is derived from the AOD at 550 nm by using the appropriate spectral scaling factor. In addition to the AOD, the single scattering albedo (SSA) and asymmetry parameter (g) for each spectral interval is used as inherent optical properties in the radiation scheme. SSA, g and the spectral dependence of AOD for the different aerosol types follow Hess et al. (1998). Single column sensitivity experiments of the direct SW radiative effect of aerosols computed using different radiation schemes available in the ALADIN-HIRLAM system are presented by Gleeson et al. (2015).

2.3. Experimental design

The influence of aerosols on the NWP forecast over Europe during the 15 day period covering the second half of April 2011 (16^{th}-30^{th}) was simulated. Series of 4-day (96-hour) forecasts starting at 00 UTC each day were run, with a model time-step of 6 minutes. An experimental domain of 300×300 points with a grid spacing of 15 km and 60 vertical levels was used. Full radiation computations were carried out every 2^{nd} time step. A Lambert Conformal Conic projection was used with the domain centre at 53 °N and 10 °E (tangent case with the reference latitude at 53 °N and the central meridian at 10 °E).

Analysis fields from the operational ECMWF IFS model were used as boundary conditions for the ALADIN-HIRLAM system; they were available at 6-hour intervals. The upper air initial state was taken from the boundary conditions and surface analysis was performed in order to initialize the forecasts. 6-hour forecasts were run at 06, 12 and 18 UTC for data assimilation continuity. The sea-surface-temperatures (SSTs) were prescribed from the ECMWF boundary conditions and kept constant during the forecast.

4 experiments were performed. An experiment excluding aerosols referred to as CNTR-LEXP, an experiment including the TEG97 aerosol climatology referred to as TEGEXP,

an experiment using the MACv1 aerosol climatology referred to as MACv1EXP and an experiment using aerosols from the MACC reanalysis referred to as MACCEXP. In MACCEXP the AOD distributions of sea salt, organic matter + sulphates, black carbon and dust were updated every 1.5 hours. The AOD distribution was fixed in time for TEGEXP and MACv1EXP.

In the non-zero aerosol experiments climatological vertical profiles (Tanre et al., 1984) were used to derive the vertical profile of the aerosol extinction coefficients for the different aerosol species from the 550 nm AODs. In MACCEXP and TEGEXP the SSA and g values followed Hess et al. (1998) whereas in MACv1EXP SSA and g originate from the MACv1 climatology (Kinne et al., 2013) and the values were used for total AOD combining different aerosol species.

2.4. Observations used to verify the forecasts

The simulated meteorological conditions from each experiment were compared to available observations over the model domain available in the ECMWF Meteorological Archival and Retrieval System (MARS) database. The comparison was performed for each day at 00, 06, 12 and 18 UTC. The number of observations of each parameter at a given time was at least 2250 over the model domain. Bilinear interpolation was used to derive the values of the parameters from the numerical forecasts at the locations of the meteorological stations. Mean biases and root mean square errors (RMSE) for a range of meteorological parameters are presented as averages over the studied time period.

The simulated downwelling SW radiation at the surface, often referred to as global horizontal irradiance (GHI) was compared to GHI measured at Baseline Surface Radiation Network (BSRN) (Ohmura et al., 1998) stations; see Figure 6 for station locations (denoted as red circles). To exclude the influence of clouds, only mean biases and RMSEs under clear sky conditions (both in the model and observations) are presented for GHI. The total number of simulated GHI values compared to observations is 336.

3. Results

3.1. Aerosol optical properties over the European region

Monthly areal averages of AOD over Europe for the three datasets used in this study are shown in Figure 1 where the European region was defined as the geographical area bounded by 10 °W to 50 °E and 35 °N to 70 °N. Each dataset shows a clear annual cycle in AOD which is lowest during Winter (December, January, February). AOD is lowest in TEG97 and highest in the MACC reanalysis. The AOD is considerably higher in the MACC reanalysis in May to July compared to the other datasets. This possibly results from the assimilation of AODs from MODIS which has been shown to overestimate AOD over Europe compared to AERONET measurements, with the annual cycle in the overestimation peaking during summer (Schaap et al., 2008). The highest monthly average AOD exceeds 0.35 in MACC but is less than 0.3 (0.2) in MACv1 (TEG97). In the MACC reanalysis, there is a strong variability in AOD over Europe not accounted for when monthly climatologies are used. The vertical bars on the MACC curve in Figure 1 show the standard deviation in the MACC AOD. During the summer months when the mean AOD exceeds 0.35, the standard deviation exceeds 0.05 (or 14%).

Area plots of annual average AOD for each of the aerosol datasets are shown in Figure 2. In general, the spatial distribution of annual average AOD agrees quite well across the datasets. The AOD is lower over Northern and Western Europe. Each dataset shows higher AODs over Southeast Europe for each season, and some months show a maximum over Central Europe. In the MACC reanalysis the AOD over Southeast Europe is higher compared to the other datasets for many months of the year. In TEG97 the AOD is much lower close to the Atlantic ocean compared to the other datasets.

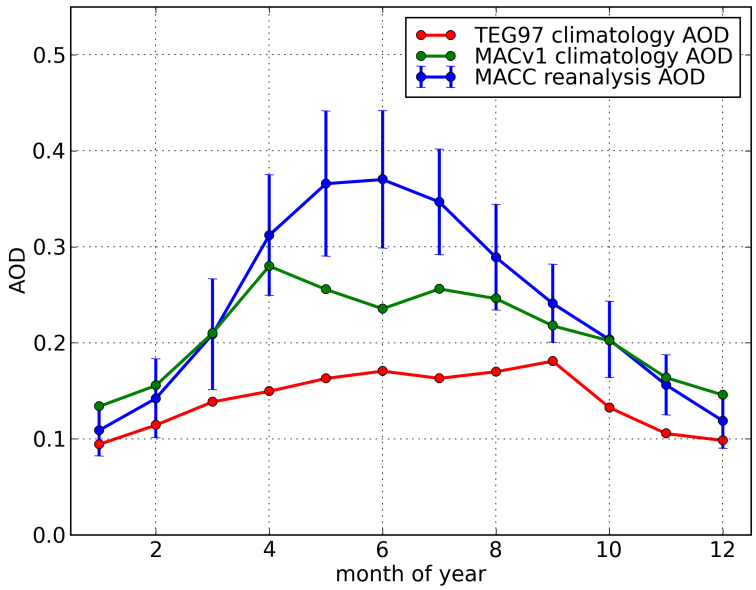

Figure 1: Monthly averages of areal averaged AOD over Europe for TEG97, MACv1 and the MACC reanalysis. The AOD standard deviation for the MACC reanalysis dataset is denoted using blue vertical bars.

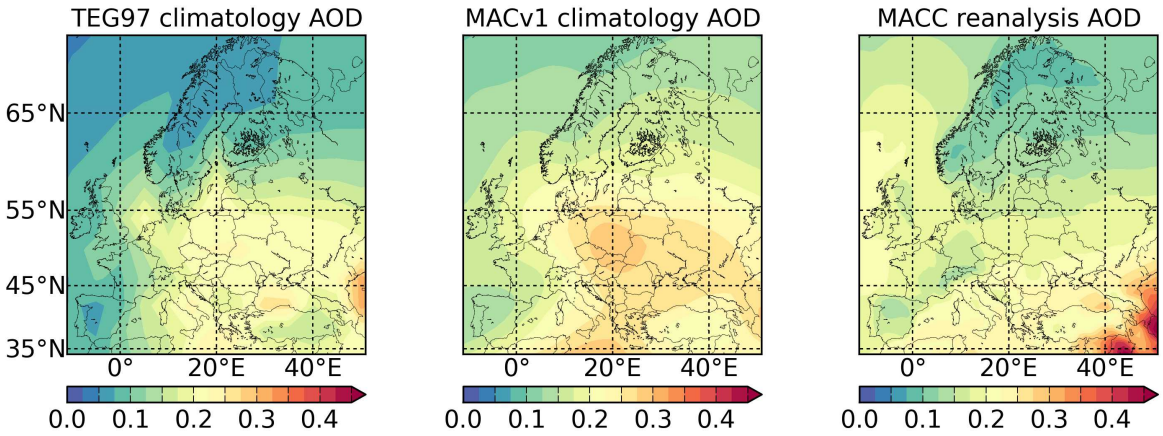

Figure 2: Annual average AOD over Europe for TEG97, MACv1 and the MACC reanalysis.

The SSA over Europe is higher in the MACv1 dataset compared to the values used in the ALADIN-HIRLAM system by default (TEG97) (Figure 3). g is lower in the MACv1 dataset (Figure 4). This results in stronger backscattering and less absorption of SW radiation when using the MACv1 climatology.

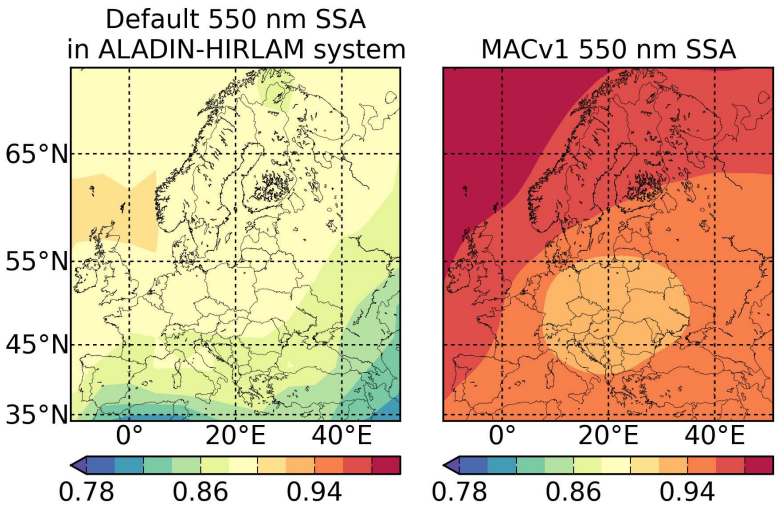

Figure 3: Default annual average SSA over Europe for the ALADIN-HIRLAM system following Hess et al. (1998) and for MACv1.

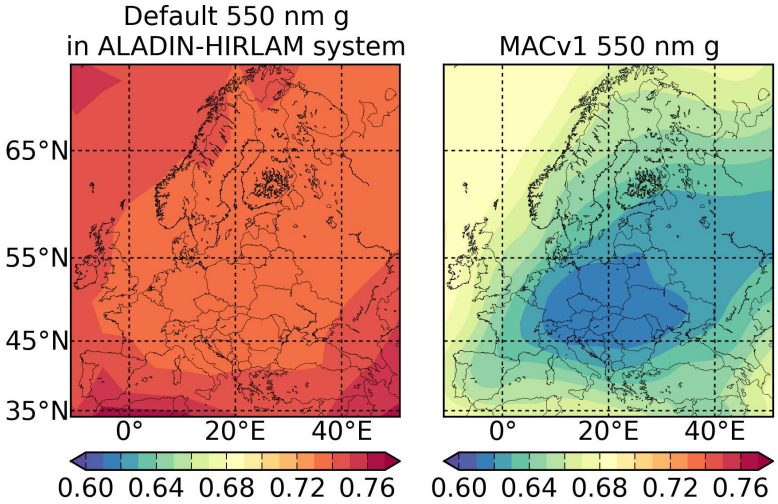

Figure 4: Default annual average g over Europe for the ALADIN-HIRLAM system following Hess et al. (1998) and for MACv1.

3.2. Modelling results

3.2.1. Simulated direct radiative effect of aerosols

The distribution of AOD determines the magnitude of the direct radiative effect of aerosols to a large extent. The AOD from different aerosol datasets for the period April 16th-30th 2011 is shown in Figure 5. AOD is lowest in the TEG97 climatology which has highest AOD values

of between 0.2 and 0.3 over Central Europe. The spatial pattern is similar in MACv1 but this dataset has maximum AOD values of up to 0.4. The MACC reanalysis values are similar to MACv1. AODs over the Atlantic coast are lower in TEG97 than in the other datasets. In MACCEXP time-varying aerosol data were used so that there are days with lower and higher AODs than the average values shown in Figure 5. The meteorological parameters shown throughout the remainder of section 3 correspond to averages over the studied time period.

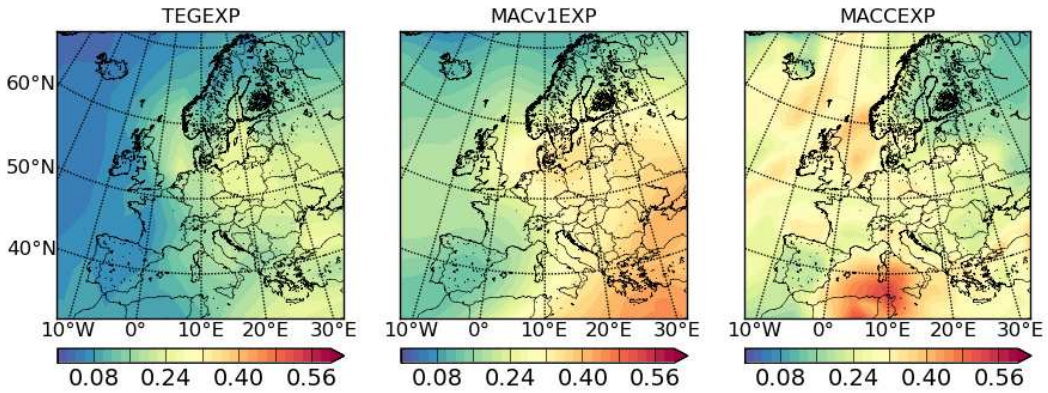

Figure 5: Average 550 nm AOD for April 16th-30th 2011 for TEG97, MACv1 and the MACC reanalysis.

The amount of SW radiation reaching the surface is decreased through the direct radiative effect of aerosols and this leads to changes in the surface energy budget. The decrease in GHI relative to the CNTRLEXP is up to 12%, 10% and 8% in MACv1EXP, MACCEXP and TEGEXP respectively (Figure 6). The decrease in GHI over the Atlantic coast compared to the CNTRLEXP is 2-4% in the TEGEXP, but is more than twice this in MACv1EXP and MACCEXP. A similar difference was seen in the AOD distribution in the different datasets. The amount of absorbed SW radiation in the atmosphere compared to the CNTRLEXP increased by up to 30%, 27.5% and 25% in MACCEXP, MACv1EXP and TEGEXP respectively (Figure 7).

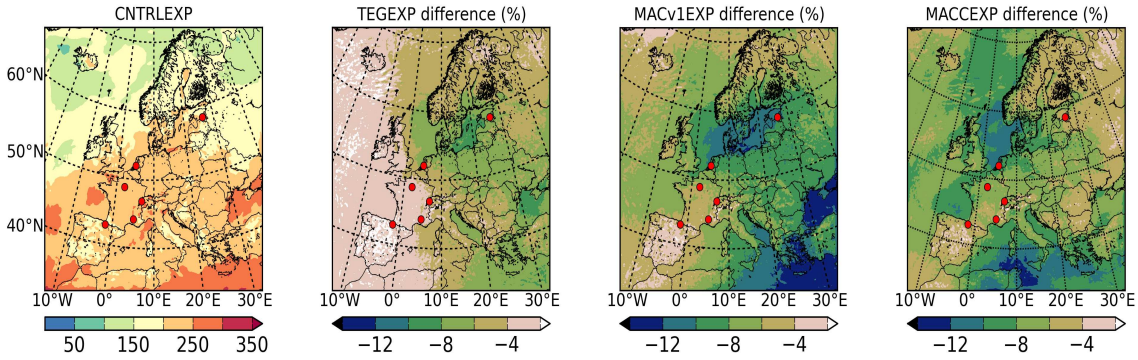

Figure 6: Daily average GHI at the surface (W/m^2) for the CNTRLEXP and the difference (%) relative to the CNTRLEXP for TEGEXP, MACv1EXP and MACCEXP. BSRN stations are denoted as red circles.

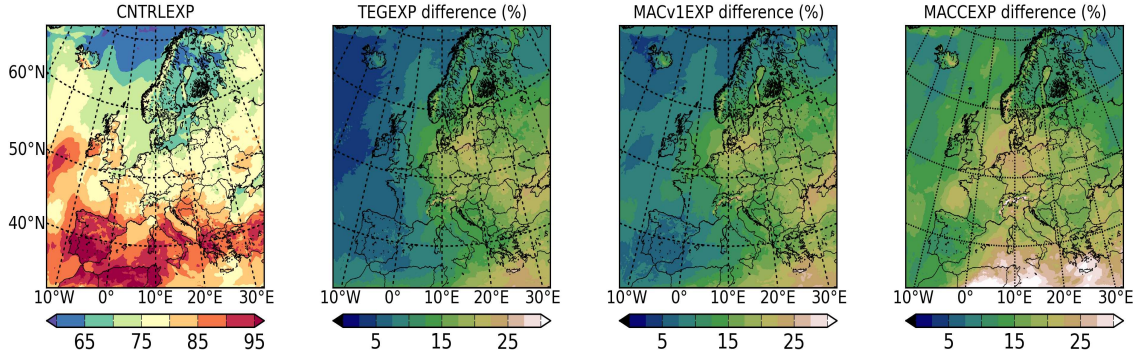

Figure 7: Daily average SW absorption rate of the atmosphere (W/m^2) for the CNTRLEXP and the difference (%) relative to the CNTRLEXP for TEGEXP, MACv1EXP and MACCEXP.

3.2.2. Influence of the direct radiative effect of aerosols on meteorological conditions

Turbulent fluxes at the surface are weakened when the direct radiative effect of aerosols is included in NWP forecasts. Changes in the turbulent fluxes over the ocean are negligible as the SSTs are taken from the ECMWF boundary conditions. Daily average sensible heat flux over land is decreased by up to 10 W/m^2, 8 W/m^2 and 6 W/m^2 in MACv1EXP, MACCEXP and TEGEXP respectively (Figure 8) compared to CNTRLEXP. Similarly, the daily average latent heat of evaporation flux at the surface over land is decreased by up to 12 W/m^2, 10 W/m^2 and 8 W/m^2 respectively (Figure 9).

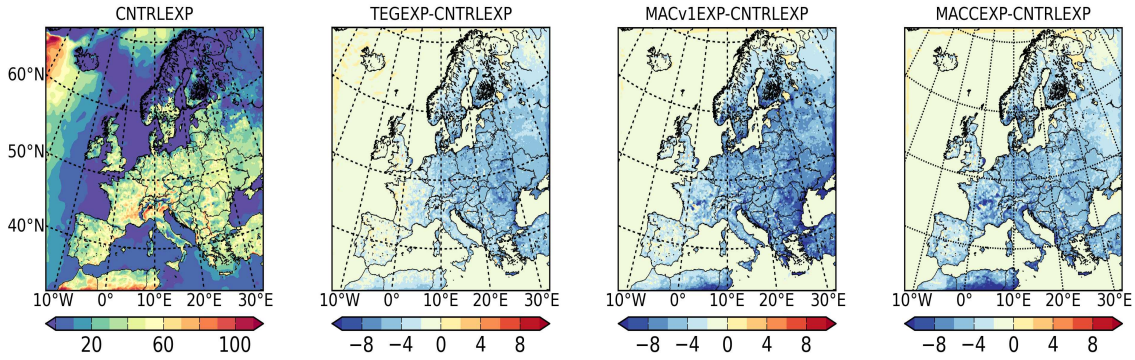

Figure 8: Daily average sensible heat flux at the surface (W/m^2) for the CNTRLEXP and the differences (W/m^2) relative to CNTRLEXP for TEGEXP, MACv1EXP and MACCEXP.

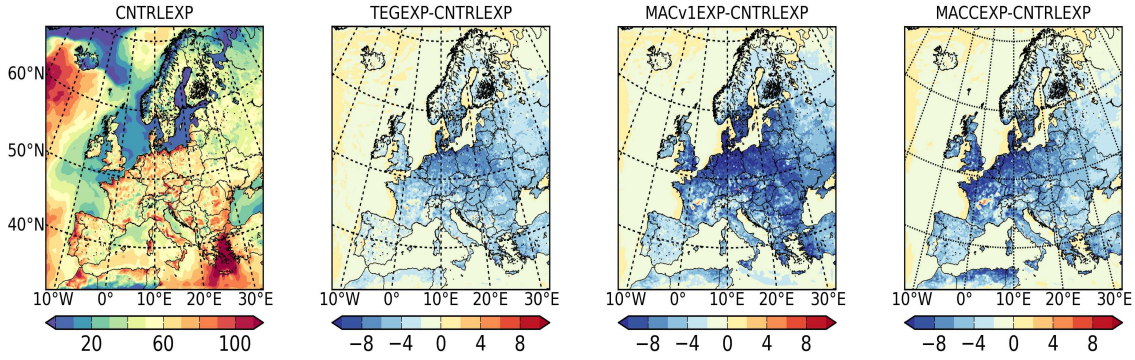

Figure 9: Daily average flux of latent heat of evaporation at the surface (W/m^2) for the CNTRLEXP and the differences (W/m^2) relative to CNTRLEXP for TEGEXP, MACv1EXP and MACCEXP.

The changes in 2 m temperatures in the aerosol-containing experiments have a different sign over the ocean than over the land. Over land 2 m temperatures are decreased due to the decrease in GHI which leads to a weakened sensible heat flux. The decrease in 2 m temperature over land compared to the CNTRLEXP is up to 0.2 °C, 0.15 °C and 0.125 °C in MACv1EXP, MACCEXP and TEGEXP respectively (Figure 10). SSTs, taken from the ECMWF boundary conditions, are kept constant during the ALADIN-HIRLAM forecasts. The diagnostic 2 m temperature is increased over the ocean due to an increase in the lowest model level temperature, caused by the increase in the amount of absorbed radiation in the aerosol containing experiments. A decrease in evaporation over land leads to a decrease in 2 m specific humidity compared to the CNTRLEXP by up to 0.2 g/kg, 0.15 g/kg and 0.10 g/kg in MACv1EXP, MACCEXP and TEGEXP respectively (Figure 11).

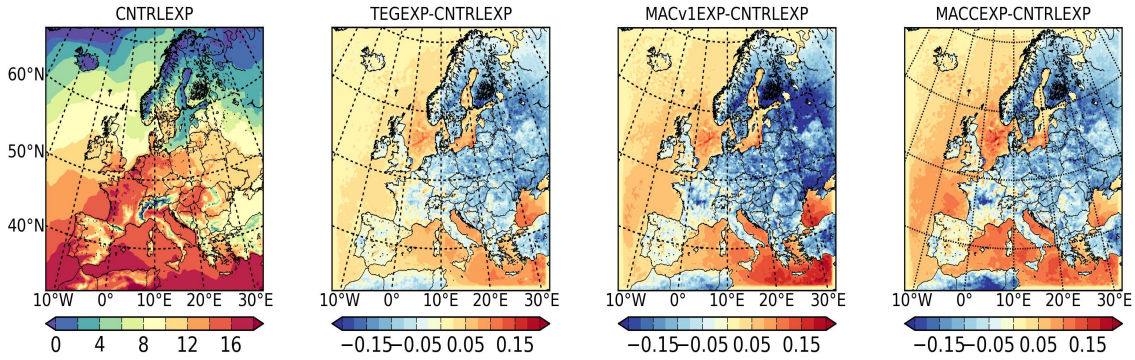

Figure 10: Daily average 2 m temperature (°C) in the CNTRLEXP and the differences (°C) relative to CNTRLEXP for TEGEXP, MACv1EXP and MACCEXP.

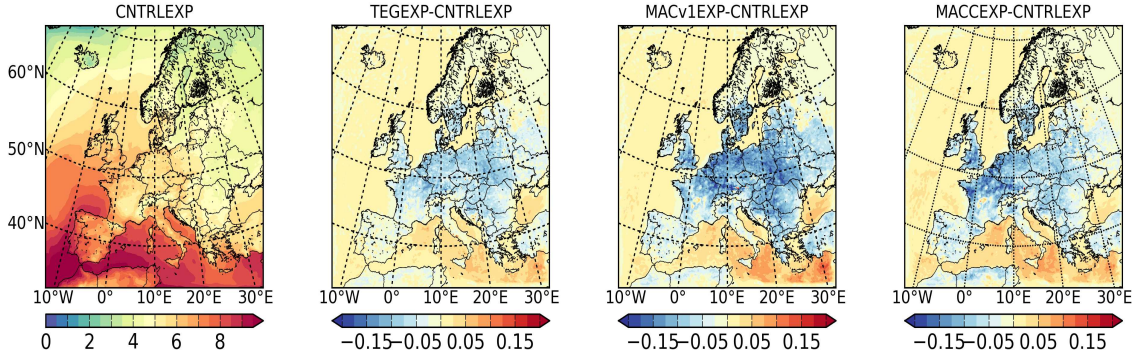

Figure 11: Daily average 2 m specific humidity (g/kg) in the CNTRLEXP and the differences (g/kg) relative to CNTRLEXP for TEGEXP, MACv1EXP and MACCEXP.

The absorption of SW radiation by aerosols leads to higher SW heating rates and higher temperatures in the lower troposphere. The average temperature over the domain increases in the 950 to 800 hPa pressure levels compared to the CNTRLEXP by 0.25 °C for MACCEXP and 0.15 °C for TEGEXP and MACv1EXP for 96 hour forecasts (Figure 12). The spatial distribution of temperature increases at the 850 hPa level for the aerosol-containing experiments are presented in Figure 13, where the highest increase is more than 0.6 °C. Increases in temperatures in the 1000 to 600 hPa layer leads to a decrease in MSLP of up to 50 Pa (Figure 14). The absorption of SW radiation, the temperature increases in the lower troposphere and the decreases in MSLP are strongest in the MACCEXP.

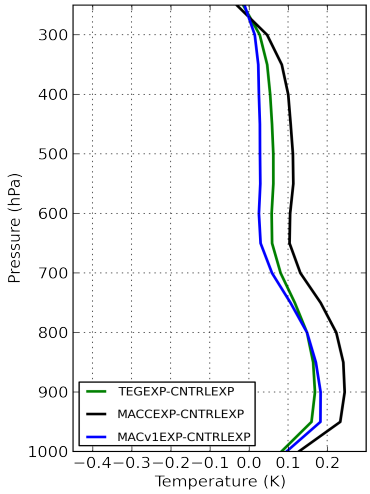

Figure 12: Domain average temperature differences (°C) on pressure levels relative to the CNTRLEXP for TEGEXP, MACv1EXP and MACCEXP for +96h forecasts.

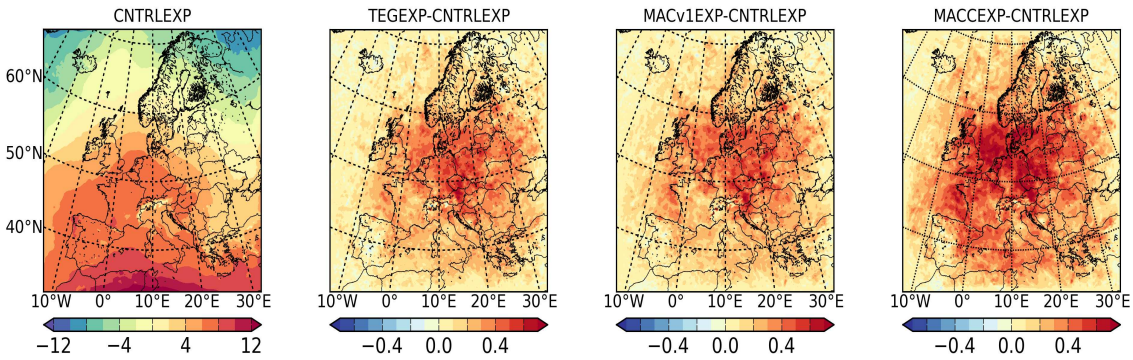

Figure 13: Average temperature (°C) on the 850 hPa pressure level in the CNTRLEXP and the differences (°C) relative to the CNTRLEXP for TEGEXP, MACv1EXP and MACCEXP for +96h forecasts.

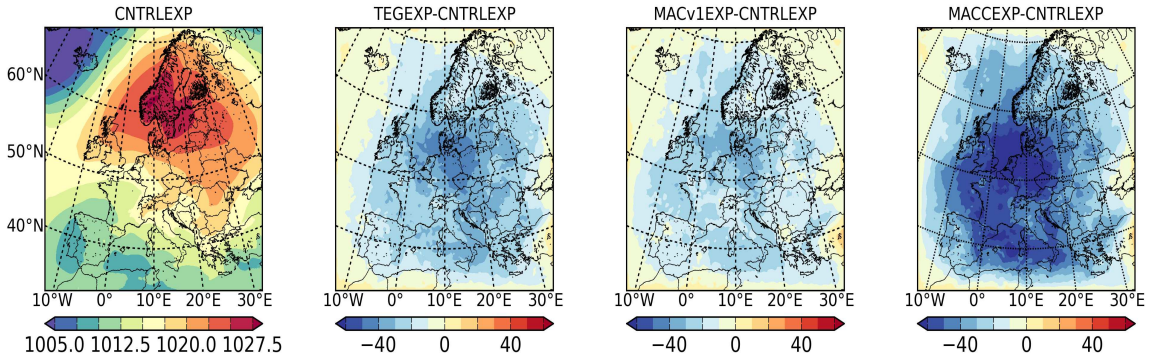

Figure 14: Average MSLP (hPa) in the CNTRLEXP and the differences (Pa) relative to CNTRLEXP for the TEGEXP, MACv1EXP and MACCEXP for +96h forecasts.

3.2.3. Influence of accounting for the direct radiative effect of aerosols on the accuracy of the NWP forecast

In general, biases and RMSEs are reduced in aerosol-containing experiments compared to the CNTRLEXP. These are presented in Table 1 for a range of meteorological parameters for each experiment, calculated at 6-hour intervals and averaged over the full forecast length (up to +96 hours). The scores are similar for each aerosol-containing experiment, but there are small improvements in MACCEXP and MACv1EXP compared to TEGEXP for forecasts of MSLP, 2 m specific humidity, cloud cover and precipitation.

The most pronounced improvements are the more accurate simulation of GHI, the temperature in the lower troposphere and the near-surface humidity. Biases and RMSEs for simulated cloud cover and precipitation are reduced. This possibly results from stabilization of the boundary layer induced by the temperature change presented in Figure 12 and from a reduction in evaporation. For 2 m temperature a cold bias of about 1 °C was detected in the CNTRLEXP. A further decrease in 2 m temperature through the direct radiative effect of aerosols over land slightly increased this cold bias.

Regarding 2 m temperature the cold bias in TEGEXP, MACv1EXP and MACCEXP increased in forecasts of length up to 60 hours but decreased in the 60-96 hour forecasts compared to the CNTRLEXP (Figure 15). There is cooling at the surface due to a decrease in the downwelling shortwave radiation reaching the surface in the aerosol containing experiments. On the other hand, aerosols absorb SW radiation in the atmosphere and this

Experiment name	CNTRLEXP	TEGEXP	MACv1EXP	MACCEXP
MSLP bias (hPa)	0.90	0.77	0.80	0.71
MSLP RMSE (hPa)	1.63	1.53	1.56	1.50
2 m temperature bias (°C)	-1.01	-1.03	-1.04	-1.03
2 m temperature RMSE (°C)	2.92	2.93	2.94	2.93
2 m specific humidity bias (g/kg)	0.16	0.13	0.10	0.12
2 m specific humidity RMSE (g/kg)	1.09	1.08	1.07	1.08
Cloud cover bias (octas)	0.50	0.43	0.41	0.42
Cloud cover RMSE (octas)	2.70	2.69	2.68	2.69
12 h precipitation bias (mm/12h)	0.25	0.21	0.19	0.19
12 h precipitation RMSE (mm/12h)	2.41	2.40	2.38	2.39
GHI bias (W/m^2)	15.07	1.49	-5.30	-2.79
GHI RMSE (W/m^2)	16.54	8.07	10.20	8.32

Table 1: RMSEs and biases for a range of meteorological parameters for CNTRLEXP, TEGEXP, MACv1EXP and MACCEXP. RMSE and bias are calculated at 6-hour intervals and averaged over the full forecast length (up to +96 hours). Clear sky conditions both in the model and observations are chosen for GHI.

results in increased heating rates. As this heat is mixed also towards the surface 2m temperature will increase. Each of the experiments started at 00 UTC. During the first day the 2m temperature is lower in aerosol containing experiments than in CNTRLEXP. Later in the forecast run heat absorbed by the aerosols accumulates in the atmosphere and then the 2m temperature is lower in the CNTRLEXP. Biases and RMSEs in 2 m specific humidity are lower in the aerosol-containing experiments throughout the 96-hour forecast (Figure 16). This bias is up to 0.3 g/kg in the CNTRLEXP but is decreased by 0.1 g/kg in MACv1EXP, and less so in TEGEXP and MACCEXP.

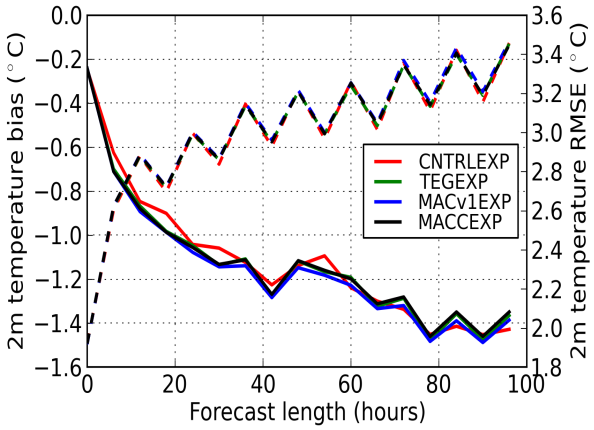

Figure 15: Bias in 2 m temperature (°C) (solid lines) and RMSE (°C) (dashed lines) for CNTRLEXP, TEGEXP, MACv1EXP and MACCEXP as a function of forecast length.

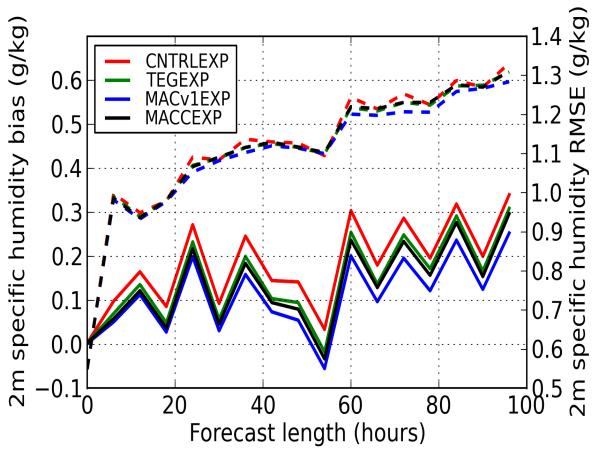

Figure 16: Bias in 2 m specific humidity (g/kg) (solid lines) and RMSE (g/kg) (dashed lines) for CNTRLEXP, TEGEXP, MACv1EXP and MACCEXP as a function of forecast length.

The negative bias and RMSE in temperature in the atmospheric layer between the 925 and 600 hPa pressure levels decreases in the aerosol-containing experiments compared to the CNTRLEXP (Figure 17). The temperature bias and RMSE at different pressure levels are lowest in MACCEXP. The MSLP bias and RMSE are reduced in the aerosol-containing experiments throughout the 96-hour forecast (Figure 18) with bias and RMSE smallest again in MACCEXP. For some meteorological parameters there is a diurnal cycle in RMSE and

bias which implies that the diurnal cycle of these meteorological parameters is not accurately resolved in the model simulations.

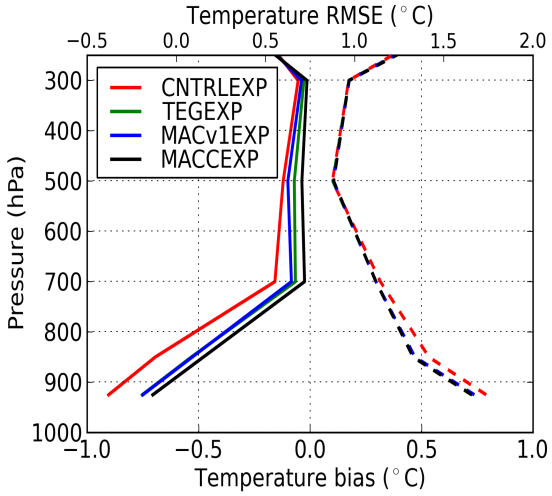

Figure 17: Average (averaged over 96-hour forecast) temperature bias (°C) (solid lines) and RMSE (°C) (dashed lines) for CNTRLEXP, TEGEXP, MACv1EXP and MACCEXP.

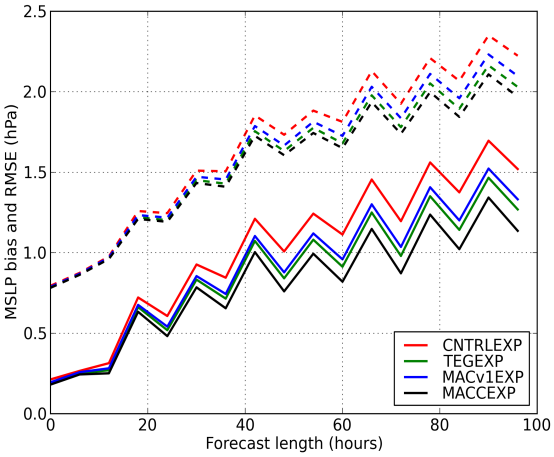

Figure 18: MSLP bias (hPa) (solid lines) and RMSE (hPa) (dashed lines) for CNTRLEXP, TEGEXP, MACv1EXP and MACCEXP as a function of forecast length.

4. Discussion

The direct radiative effect of aerosols over the European region was studied for April 2011. The magnitude of the effect may be different for other years and months due to the

seasonal cycle and variability of AOD. However, a similar sensitivity of the meteorological response is expected. In addition, the temperature and humidity bias in NWP forecasts over Europe may be season dependent and the influence of considering the direct radiative effect of aerosols may have different impacts on the forecast accuracy in different seasons. The distribution of AOD in the different datasets for the period studied was similar to the annual average distribution in the respective aerosol datasets. The presented modelling results are expected to be representative for the periods where aerosol distributions are close to average (as was the studied period), but not for the situations with extremely high AODs.

Extensive verification of the meteorological forecasts was performed and in the different aerosol-containing experiments the meteorological forecasts were more accurate compared to the CNTRLEXP which did not include aerosols. This illustrates the importance of including the direct radiative effect of aerosols in NWP models. The most important benefits include the improved simulation of SW radiation and temperature and humidity in the lower troposphere. Using an updated climatology or time varying realistic aerosol data from reanalysis can provide small improvements compared to the default climatology in the ALADIN-HIRLAM system for the case where aerosol distributions are close to average i.e. the AOD is not extremely high. However, as has been previously shown by Toll et al. (2015) ALADIN-HIRLAM weather forecasts over Europe during events with very high AOD can be considerably improved, by considering the direct radiative effect of realistic aerosol distributions.

Improved simulation of GHI in the ALADIN-HIRLAM system is of potential interest for the solar energy community, as NWP models are the best tools to provide forecasts from 6 hours to several days ahead (Lorenz et al., 2015). In addition to improved simulation of GHI, the separation between the diffuse and direct fractions of GHI is important for solar energy applications. Further studies on the impact of aerosols on the direct normal irradiance (DNI) at the surface using the ALADIN-HIRLAM system are planned. The direct radiative effect of aerosols has a stronger influence on DNI than on GHI, as the diffuse fraction of SW radiation is increased when the direct fraction is decreased (Ruiz-Arias et al., 2014).

In each ALADIN-HIRLAM experiment SSTs were taken from ECMWF boundary conditions and thus kept constant. This led to negligible changes in surface turbulent fluxes

over the ocean compared to the CNTRLEXP and resulted in very different responses in near-surface temperature and humidity over the ocean compared to over land.

Here only the direct radiative effect of aerosols over Europe was studied; in the future a study of the influence of the indirect effects of aerosols in NWP forecasts is also planned.

5. Conclusions

The annual cycle of AOD over Europe is similar for the TEG97 aerosol climatology, MACv1 aerosol climatology and MACC reanalysis with lowest AODs during the winter months. Highest AODs were found in the MACC reanalysis and the lowest in the TEG97 climatology, with a general increase in AOD towards Southeast Europe. In TEG97 the AOD over the Atlantic ocean is lower than in the other datasets.

Considering the direct radiative effect of aerosols over Europe was shown to improve the accuracy of simulated radiative fluxes and the forecast of temperature and humidity in the lower troposphere.The GHI is decreased in aerosol containing experiments leading to decreased surface turbulent fluxes over land and SW heating rates are increased due to absorption of SW radiation by aerosols. More accurate simulation of GHI is important for solar energy applications. Decreases in GHI were up to 12% in the aerosol-containing experiments which led to decreases in 2 m temperature over land and weakened turbulent fluxes. The amount of absorbed SW radiation in the atmosphere was increased by up to 30% leading to higher temperatures in the lower troposphere. However, the studied time period was rather short and longer multi-annual experiments are planned in future studies in order to further evaluate the impacts of considering the direct radiative effect of aerosols over Europe on NWP forecast accuracy.

There was a rather weak dependency of the meteorological forecast on the aerosol dataset used. This implies that the TEG97 aerosol climatology, MACv1 aerosol climatology and MACC reanalysis are similar in their ability to account for the direct radiative effect of aerosols in NWP forecasts over Europe. The influence of using real-time aerosol data and the inclusion of the indirect effects of aerosols in NWP over Europe should be further studied.

Acknowledgements

We acknowledge the support of the International HIRLAM-B and ALADIN programmes. This work was supported by research grant No. 9140 from the Estonian Science Foundation and by institutional research funding IUT20-11 from the Estonian Ministry of Education and Research. We acknowledge the use of ECMWF's computing and archive facilities for this research. Aerosol data from Max-Planck-Institute Aerosol Climatology version 1 and Monitoring Atmospheric Composition and Climate reanalysis datasets and radiation measurements from the Baseline Surface Radiation Network were used.

References

Baklanov, A., Schlünzen, K., Suppan, P., Baldasano, J., Brunner, D., Aksoyoglu, S., Carmichael, G., Douros, J., Flemming, J., Forkel, R., et al., 2014. Online coupled regional meteorology chemistry models in Europe: current status and prospects. Atmospheric Chemistry and Physics 14 (1), 317–398.

Bellouin, N., Boucher, O., Haywood, J., Reddy, M. S., 2005. Global estimate of aerosol direct radiative forcing from satellite measurements. Nature 438 (7071), 1138–1141.

Benedetti, A., Morcrette, J.-J., Boucher, O., Dethof, A., Engelen, R., Fisher, M., Flentje, H., Huneeus, N., Jones, L., Kaiser, J., et al., 2009. Aerosol analysis and forecast in the European centre for medium-range weather forecasts integrated forecast system: 2. Data assimilation. Journal of Geophysical Research: Atmospheres (1984–2012) 114 (D13).

Breitkreuz, H., Schroedter-Homscheidt, M., Holzer-Popp, T., Dech, S., 2009. Short-range direct and diffuse irradiance forecasts for solar energy applications based on aerosol chemical transport and numerical weather modeling. Journal of Applied Meteorology and Climatology 48 (9), 1766–1779.

Carmona, I., Kaufman, Y., Alpert, P., 2008. Using numerical weather prediction errors to estimate aerosol heating. Tellus B 60 (5), 729–741.

399 Catry, B., Geleyn, J.-F., Bouyssel, F., Cedilnik, J., Brožková, R., Derková, M., et al., 2008.
400 A new sub-grid scale lift formulation in a mountain drag parameterisation scheme. Mete-
401 orologische Zeitschrift 17 (2), 193–208.

402 Catry, B., Geleyn, J.-F., Tudor, M., Bénard, P., Trojáková, A., 2007. Flux-conservative
403 thermodynamic equations in a mass-weighted framework. Tellus A 59 (1), 71–79.

404 Clough, S., Shephard, M., Mlawer, E., Delamere, J., Iacono, M., Cady-Pereira, K., Bouk-
405 abara, S., Brown, P., 2005. Atmospheric radiative transfer modeling: a summary of the
406 AER codes. Journal of Quantitative Spectroscopy and Radiative Transfer 91, 233–244.

407 Cook, J., Highwood, E., 2004. Climate response to tropospheric absorbing aerosols in an
408 intermediate general-circulation model. QJR Meteorol. Soc 130 (596), 175–191.

409 Davies, H., 1976. A lateral boundary formulation for multi-level prediction models. Quarterly
410 Journal of the Royal Meteorological Society 102, 405–418.

411 Flemming, J., Inness, A., Flentje, H., Huijnen, V., Moinat, P., Schultz, M., Stein, O., 2009.
412 Coupling global chemistry transport models to ECMWF's integrated forecast system. Geo-
413 scientific Model Development 2, 253–265.

414 Fouquart, Y., Bonnel, B., 1980. Computations of solar heating of the earth's atmosphere- A
415 new parameterization. Beitraege zur Physik der Atmosphaere 53, 35–62.

416 Garcıa, O., Dıaz, J., Expósito, F., Dıaz, A., Dubovik, O., Derimian, Y., Dubuisson, P., Roger,
417 J., 2012. Shortwave radiative forcing and efficiency of key aerosol types using AERONET
418 data. Atmos. Chem. Phys 12, 5129–5145.

419 Geleyn, J.-F., Catry, B., Bouteloup, Y., Brožková, R., 2008. A statistical approach for sedi-
420 mentation inside a microphysical precipitation scheme. Tellus A 60 (4), 649–662.

421 Geleyn, J.-F., Váňa, F., Cedilnik, J., Tudor, M., Catry, B., 2006. An intermediate solu-
422 tion between diagnostic exchange coefficients and prognostic TKE methods for vertical
423 turbulent transport. WGNE Blue Book, 2 pp.

Gerard, L., Piriou, J.-M., Brožková, R., Geleyn, J.-F., Banciu, D., 2009. Cloud and Precipitation Parameterization in a Meso-Gamma-Scale Operational Weather Prediction Model. Monthly Weather Review 137, 3960–3977.

Gleeson, E., Toll, V., Nielsen, K., Rontu, L., Mašek, J., 2015. Effects of aerosols on solar radiation in the ALADIN-HIRLAM NWP system. Atmospheric Chemistry and Physics Discussions 15 (22), 32519–32560.

Grell, G., Baklanov, A., 2011. Integrated modeling for forecasting weather and air quality: A call for fully coupled approaches. Atmospheric Environment 45 (38), 6845–6851.

Haugen, J., Machenhauer, B., 1993. A Spectral Limited-Area Model Formulation with Time-dependent Boundary Conditions Applied to the Shallow-Water Equations. Monthly Weather Review 121, 2618–2630.

Haywood, J., Boucher, O., 2000. Estimates of the direct and indirect radiative forcing due to tropospheric aerosols: A review. Reviews of Geophysics - Richmond Virginia then Washington 38 (4), 513–543.

Hess, M., Koepke, P., Schult, I., 1998. Optical properties of aerosols and clouds: The software package OPAC. Bulletin of the American meteorological society 79 (5), 831–844.

Hohenegger, C., Vidale, P. L., 2005. Sensitivity of the European climate to aerosol forcing as simulated with a regional climate model. Journal of Geophysical Research: Atmospheres (1984–2012) 110 (D6).

Holben, B., Eck, T., Slutsker, I., Tanre, D., Buis, J., Setzer, A., Vermote, E., Reagan, J., Kaufman, Y., Nakajima, T., et al., 1998. AERONET — A federated instrument network and data archive for aerosol characterization. Remote sensing of environment 66 (1), 1–16.

Hortal, M., 2002. The development and testing of a new two-time-level semi-Lagrangian scheme (SETTLS) in the ECMWF forecast model. Quarterly Journal of the Royal Meteorological Society 128, 1671–1687.

Inness, A., Baier, F., Benedetti, A., Bouarar, I., Chabrillat, S., Clark, H., Clerbaux, C., Coheur, P., Engelen, R., Errera, Q., et al., 2013. The MACC reanalysis: an 8 yr data set of atmospheric composition. Atmospheric chemistry and physics 13, 4073–4109.

Jacobson, M. Z., et al., 2001. Global direct radiative forcing due to multicomponent anthropogenic and natural aerosols. Journal of Geophysical Research 106 (D2), 1551–1568.

Joseph, J. H., Wiscombe, W., Weinman, J., 1976. The delta-Eddington approximation for radiative flux transfer. Journal of the Atmospheric Sciences 33 (12), 2452–2459.

Kinne, S., O'Donnel, D., Stier, P., Kloster, S., Zhang, K., Schmidt, H., Rast, S., Giorgetta, M., Eck, T. F., Stevens, B., 2013. MAC-v1: a new global aerosol climatology for climate studies. Journal of Advances in Modeling Earth Systems 5 (4), 704–740.

Lindstedt, D., Lind, P., Kjellström, E., Jones, C., 2015. A new regional climate model operating at the meso-gamma scale: performance over Europe. Tellus A 67.

Loeb, N. G., Manalo-Smith, N., 2005. Top-of-atmosphere direct radiative effect of aerosols over global oceans from merged CERES and MODIS observations. Journal of Climate 18 (17), 3506–3526.

Lorenz, E., Heinemann, D., Kuehnert, J., Nielsen, K., Remund, J., Mueller, S., 2015. Comparison of irradiance forecasts based on numerical weather prediction models with different spatio-temporal resolutions (in review). Progress in Photovoltaics: Research and Applications.

Mascart, P., Bougeault, P., 2011. The Meso-NH atmospheric simulation system: Scientific documentation. Tec h. rep., Meteo France, Toulouse, France.

Masson, V., Le Moigne, P., Martin, E., Faroux, S., Alias, A., Alkama, R., Belamari, S., Barbu, A., Boone, A., Bouyssel, F., et al., 2013. The SURFEXv7.2 land and ocean surface platform for coupled or offline simulation of earth surface variables and fluxes, geosci. model dev., 6, 929–960, doi: 10.5194.

Milton, S., Greed, G., Brooks, M., Haywood, J., Johnson, B., Allan, R., Slingo, A., Grey, W., 2008. Modeled and observed atmospheric radiation balance during the West African dry season: Role of mineral dust, biomass burning aerosol, and surface albedo. Journal of Geophysical Research: Atmospheres (1984–2012) 113 (D23).

Mlawer, E. J., Taubman, S. J., Brown, P. D., Iacono, M. J., Clough, S. A., 1997. Radiative transfer for inhomogeneous atmospheres: RRTM, a validated correlated-k model for the longwave. Journal of Geophysical Research: Atmospheres (1984–2012) 102 (D14), 16663–16682.

Morcrette, J.-J., Benedetti, A., Ghelli, A., Kaiser, J., Tompkins, A., 2011. Aerosol-Cloud-Radiation Interactions and their Impact on ECMWF/MACC Forecasts. ECMWF Technical Memorandum 660.

Morcrette, J.-J., Boucher, O., Jones, L., Salmond, D., Bechtold, P., Beljaars, A., Benedetti, A., Bonet, A., Kaiser, J., Razinger, M., et al., 2009. Aerosol analysis and forecast in the European Centre for medium-range weather forecasts integrated forecast system: Forward modeling. Journal of Geophysical Research: Atmospheres (1984–2012) 114 (D6).

Mulcahy, J., Walters, D., Bellouin, N., Milton, S., 2014. Impacts of increasing the aerosol complexity in the Met Office global numerical weather prediction model. Atmos. Chem. Phys 14, 4749–4778.

Myhre, G., Samset, B., Schulz, M., Balkanski, Y., Bauer, S., Berntsen, T., Bian, H., Bellouin, N., Chin, M., Diehl, T., et al., 2013. Radiative forcing of the direct aerosol effect from AeroCom phase II simulations. Atmospheric Chemistry and Physics 13, 1853–1877.

Nabat, P., Somot, S., Mallet, M., Chiapello, I., Morcrette, J., Solmon, F., Szopa, S., Dulac, F., Collins, W., Ghan, S., et al., 2013. A 4-D climatology (1979–2009) of the monthly tropospheric aerosol optical depth distribution over the Mediterranean region from a comparative evaluation and blending of remote sensing and model products. Atmospheric Measurement Techniques 6 (5), 1287–1314.

Nielsen, K. P., Gleeson, E., Rontu, L., 2014. Radiation sensitivity tests of the HARMONIE 37h1 NWP model. Geoscientific Model Development 7 (4), 1433–1449.

Ohmura, A., Gilgen, H., Hegner, H., Müller, G., Wild, M., Dutton, E. G., Forgan, B., Fröhlich, C., Philipona, R., Heimo, A., et al., 1998. Baseline Surface Radiation Network (BSRN/WCRP): New precision radiometry for climate research. Bulletin of the American Meteorological Society 79 (10), 2115–2136.

Palamarchuk, I., Ivanov, S., Ruban, I., Pavlova, H., 2016. Influence of aerosols on atmospheric variables in the HARMONIE model. Atmospheric Research 169, 539–546.

Pérez, C., Nickovic, S., Pejanovic, G., Baldasano, J. M., Özsoy, E., 2006. Interactive dust-radiation modeling: A step to improve weather forecasts. Journal of Geophysical Research: Atmospheres (1984–2012) 111 (D16).

Reale, O., Lau, K., da Silva, A., 2011. Impact of interactive aerosol on the African Easterly Jet in the NASA GEOS-5 global forecasting system. Weather and forecasting 26 (4), 504–519.

Rodwell, M. J., Jung, T., 2008. Understanding the local and global impacts of model physics changes: An aerosol example. Quarterly Journal of the Royal Meteorological Society 134 (635), 1479–1497.

Ruiz-Arias, J., Dudhia, J., Gueymard, C., 2014. A simple parameterization of the short-wave aerosol optical properties for surface direct and diffuse irradiances assessment in a numerical weather model. Geoscientific Model Development 7 (3), 1159–1174.

Simmons, A., Burridge, D., 1981. An Energy and Angular-Momentum Conserving Vertical Finite-Difference Scheme and Hybrid Vertical Coordinates. Monthly Weather Review 109, 758–766.

Stamnes, K., Tsay, S.-C., Wiscombe, W., Jayaweera, K., et al., 1988. Numerically stable algorithm for discrete-ordinate-method radiative transfer in multiple scattering and emitting layered media. Applied optics 27 (12), 2502–2509.

Takemura, T., Nozawa, T., Emori, S., Nakajima, T. Y., Nakajima, T., 2005. Simulation of climate response to aerosol direct and indirect effects with aerosol transport-radiation model. Journal of Geophysical Research: Atmospheres (1984–2012) 110 (D2).

Tanre, D., Geleyn, J., Slingo, J., 1984. First results of the introduction of an advanced aerosol-radiation interaction in the ECMWF low resolution global model. Aerosols and their climatic effects, 133–177.

Tegen, I., Hollrig, P., Chin, M., Fung, I., Jacob, D., Penner, J., 1997. Contribution of different aerosol species to the global aerosol extinction optical thickness: Estimates from model results. Journal of Geophysical Research: Atmospheres (1984–2012) 102 (D20), 23895–23915.

Temperton, C., Staniforth, A., 1987. An Efficient Two-Time-Level Semi-Lagrangian Semi-Implicit Integration Scheme. Quarterly Journal of the Royal Meteorological Society 113, 1025–1039.

Toll, V., Reis, K., Ots, R., Kaasik, M., Männik, A., Prank, M., Sofiev, M., 2015. SILAM and MACC reanalysis aerosol data used for simulating the aerosol direct radiative effect with the NWP model HARMONIE for summer 2010 wildfire case in Russia. Atmospheric Environment.

Tompkins, A., Cardinali, C., Morcrette, J.-J., Rodwell, M., 2005. Influence of aerosol climatology on forecasts of the African Easterly Jet. Geophysical research letters 32 (10).

Untch, A., Hortal, M., 2004. A finite-element scheme for the vertical discretization of the semi-Lagrangian version of the ECMWF forecast model. Quarterly Journal of the Royal Meteorological Society 130, 1505–1530.

Váňa, F., Bénard, P., Geleyn, J.-F., Simon, A., Seity, Y., 2008. Semi-Lagrangian advection scheme with controlled damping: An alternative to nonlinear horizontal diffusion in a numerical weather prediction model. Quarterly Journal of the Royal Meteorological Society 134, 523–537.

552 Wang, C., 2004. A modeling study on the climate impacts of black carbon aerosols. Journal
553 of Geophysical Research: Atmospheres (1984–2012) 109 (D3).

554 White, P., 2004. IFS documentation (CY23R4), part IV: Physical processes.

555 Xu, K.-M., Randall, D., 1996. A Semiempirical Cloudiness Parameterization for Use in Cli-
556 mate Models. Journal of the Atmospheric Sciences 53 (21), 3084–3102.

557 Yu, H., Kaufman, Y., Chin, M., Feingold, G., Remer, L., Anderson, T., Balkanski, Y.,
558 Bellouin, N., Boucher, O., Christopher, S., et al., 2006. A review of measurement-based
559 assessments of the aerosol direct radiative effect and forcing. Atmospheric Chemistry and
560 Physics 6 (3), 613–666.

561 Zamora, R. J., Dutton, E. G., Trainer, M., McKeen, S. A., Wilczak, J. M., Hou, Y.-T.,
562 2005. The accuracy of solar irradiance calculations used in mesoscale numerical weather
563 prediction. Monthly weather review 133 (4), 783–792.

564 Zhang, Y., 2008. Online-coupled meteorology and chemistry models: history, current status,
565 and outlook. Atmospheric Chemistry and Physics 8 (11), 2895–2932.

566 Zubler, E., Lohmann, U., Lüthi, D., Schär, C., 2011. Intercomparison of aerosol climatologies
567 for use in a regional climate model over Europe. Geophysical Research Letters 38 (15).